J. Fluid Mech. (2001), *vol.* 444, *pp.* 199–221. Printed in the United Kingdom

Verification of Hasselmann's energy transfer among surface gravity waves by direct numerical simulations of primitive equations

By MITSUHIRO TANAKA

Department of Civil Engineering, Faculty of Engineering, Gifu University,
1-1 Yanagido, Gifu 501-1193, Japan

(Received 24 August 2000 and in revised form 2 April 2001)

The temporal evolution of nonlinear wave fields of surface gravity waves is studied by large-scale direct numerical simulations of primitive equations in order to verify Hasselmann's theory for nonlinear energy transfer among component gravity waves. In the simulations, all the nonlinear interactions, including both resonant and non-resonant ones, are taken into account up to the four-wave processes. The initial wave field is constructed by combining more than two million component free waves in such a way that it has the JONSWAP or the Pierson–Moskowitz spectrum. The nonlinear energy transfer is evaluated from the rate of change of the spectrum, and is compared with Hasselmann's theory. It is shown that, in spite of apparently insufficient duration of the simulations such as just a few tens of characteristic periods, the energy transfer obtained by the present method shows satisfactory agreement with Hasselmann's theory, at least in their qualitative features.

1. Introduction

The ocean waves are usually described, at least to lowest-order approximation, as a superposition of an infinite number of component waves with various amplitudes, frequencies and directions of propagation. These component waves interact with each other through the nonlinearity of the governing equations and the boundary conditions at the free surface, and also interact with the turbulent air flow blowing above them as well as the turbulent motion within the water. In order to describe such a complicated system with infinitely many degrees of freedom, we usually abandon the deterministic description and resort instead to a statistical description. Among various statistical quantities which are used to describe the state of the ocean wave field, one of the most important and informative quantities is the energy spectrum which expresses how the energy of the ocean wave field is distributed among component waves. In terms of the wavenumber spectrum $\epsilon(\boldsymbol{k})$ or the directional spectrum $\Phi(\omega, \theta)$, the energy density E (i.e. the energy of the wave field per unit horizontal area) is expressed as

$$E = \int \epsilon(\boldsymbol{k})\,\mathrm{d}\boldsymbol{k} = \int_0^{2\pi} \int_0^{\infty} \Phi(\omega, \theta)\,\mathrm{d}\omega\,\mathrm{d}\theta, \tag{1.1}$$

where $\boldsymbol{k}$ is the two-dimensional wavenumber vector in the horizontal plane, ω is the linear frequency defined as $\omega(\boldsymbol{k}) = (g|\boldsymbol{k}|)^{1/2}$, and θ is the direction of propagation. The

frequency spectrum $\Psi(\omega)$ can be obtained by integrating $\Phi(\omega, \theta)$ with respect to θ:

$$\Psi(\omega) = \int_0^{2\pi} \Phi(\omega, \theta)\, \mathrm{d}\theta. \tag{1.2}$$

At present, the energy spectrum of the ocean wave field is considered to evolve in space and time according to the 'energy balance equation':

$$\frac{\partial \epsilon(\boldsymbol{k}; \boldsymbol{x}, t)}{\partial t} + \boldsymbol{c}_g(\boldsymbol{k}) \cdot \nabla_h \epsilon(\boldsymbol{k}; \boldsymbol{x}, t) = S_{nl} + S_{in} + S_{ds}, \tag{1.3}$$

where ∇_h denotes the gradient operator in the horizontal $\boldsymbol{x}$-plane and $\boldsymbol{c}_g(\boldsymbol{k})$ is the vector group velocity. This equation is also called the 'kinetic wave equation'. The source terms S_{nl}, S_{in} and S_{ds} represent, respectively, the energy transfer between different component waves due to nonlinearity, energy input from the wind, and the energy dissipation due to white capping. Among those source terms, we will focus our attention here on S_{nl}. For S_{nl}, Hasselmann (1962) has derived a complicated yet explicit expression:

$$S_{nl}(\boldsymbol{k}_4) = \iiint \omega_4 |T_{1234}|^2 \delta(\boldsymbol{k}_1 + \boldsymbol{k}_2 - \boldsymbol{k}_3 - \boldsymbol{k}_4) \delta(\omega_1 + \omega_2 - \omega_3 - \omega_4) \times \{N_1 N_2 (N_3 + N_4) - N_3 N_4 (N_1 + N_2)\}\, \mathrm{d}\boldsymbol{k}_1\, \mathrm{d}\boldsymbol{k}_2\, \mathrm{d}\boldsymbol{k}_3. \tag{1.4}$$

Here $N(\boldsymbol{k})$ is the wave action density defined as $N(\boldsymbol{k}) = \epsilon(\boldsymbol{k})/\omega(\boldsymbol{k})$, $\omega_i = \omega(\boldsymbol{k}_i)\,(i = 1, 2, 3, 4)$, T_{1234} is a complicated function of $\boldsymbol{k}_1$, $\boldsymbol{k}_2$, $\boldsymbol{k}_3$, $\boldsymbol{k}_4$, and δ is Dirac's delta function. When the wave field is statistically homogeneous, and both S_{in} and S_{ds} are absent, (1.3) is greatly simplified to become

$$\frac{\partial \epsilon(\boldsymbol{k}; t)}{\partial t} = S_{nl}, \tag{1.5}$$

and this is the form of the energy balance equation which we shall deal with in this study.

Hasselmann (1962) obtained the expression (1.4) for S_{nl} by applying a perturbation analysis to the primitive equations for surface gravity waves which are described in terms of surface displacement $\eta(\boldsymbol{x}, t)$ and velocity potential $\phi(\boldsymbol{x}, z, t)$. Zakharov (1968) formulated the same problem of nonlinear surface water waves as a Hamiltonian system and derived an evolution equation for the complex amplitude of component waves which is now known as the Zakharov equation. By way of this equation, the derivation procesure of S_{nl} can be made much simpler and theoretically more transparent than the original method of Hasselmann. For detailed derivation of the kinetic equation from the Zakharov equation, see, for example, Zakharov (1999), Zakharov, L'vov & Falkovich (1992), and Yuen & Lake (1982). Dyachenko & Lvov (1995) have confirmed that the expression for S_{nl} which has been derived from the Zakharov equation is equivalent to Hasselmann's original expression (1.4).

Many researchers have taken the validity of the expression (1.4) for granted and have been trying to develop efficient numerical algorithms which evaluate it fast enough to be used in wave forecasting routinely. However, when we review the derivation of the expression (1.4) for S_{nl}, there are several points to feel uneasy about. For example,

(*a*) Hasselmann's S_{nl}, as well as the Zakharov equation, has been derived for wave fields with broad-band spectra, and hence all the component waves are assumed to

have energy of the same order of magnitude. Therefore the asymptotic relation

$$b(\boldsymbol{k}_1) \gg b(\boldsymbol{k}_2)\, b(\boldsymbol{k}_3) \gg b(\boldsymbol{k}_4)\, b(\boldsymbol{k}_5)\, b(\boldsymbol{k}_6) \tag{1.6}$$

is assumed to hold for any combination of wavenumbers $\boldsymbol{k}_i$. Here $b(\boldsymbol{k})$ is the complex amplitude function introduced by Zakharov (1968) and is reviewed briefly in the next section. On the other hand, in a typical wind wave field, the energy spectrum is known to decay like ω^{-m} with $m = 4$–5. Then the amplitudes of component waves whose frequencies are larger than twice the peak frequency are only several percent of that of the peak mode at the most. Therefore an asymptotic relation like (1.6) does not necessarily hold in the actual ocean wave field.

(*b*) Hasselmann's theory predicts that the nonlinear energy transfer occurs only among those waves which satisfy resonance conditions exactly, while all the other off-resonant interactions do not contribute to the evolution of the spectrum at all. In the derivation of (1.4) from the Zakharov equation, this exclusive selection of resonant interactions is achieved as a result of integration with respect to t over a time scale much longer than $(ak)^{-2}$, with ak being a small parameter measuring the characteristic 'steepness' of the wave field. If we take this fact naively, the derivation procedure appears to imply that the change of the spectrum due to resonant interactions can be observed only after we take a temporal average over many hundred characteristic periods of the wave field. Should this be the case, what happens if we trace the evolution of the wave field deterministically for a much shorter time, say just a few tens of periods, and estimate the change of the spectrum of the field? Can we still observe any sensible energy transfer comparable to Hasselmann's S_{nl}, or do the lower-order, hence stronger, non-resonant interactions, whose effect would not cancel out enough in such a short interval of time, mask the net energy transfer due to the four-wave process? If it turns out that we cannot detect the energy transfer due to four-wave resonant interactions from such a short deterministic evolution, what is the relevance of the kinetic equation (1.5) for such a short-term or mid-term evolution of the wave field?

With these considerations in mind, we believe that the validity of Hasselmann's expression for S_{nl} needs to be critically assessed by some completely independent measure. We do not think it a sound situation that, although Hasselmann's S_{nl} has never been confirmed by any independent measure, nevertheless everybody believes in it. It is clear that verification of Hasselmann's theory can never be achieved in field observations, where effects of other sources such as S_{in} and S_{ds} are always present. Zhao *et al.* (1996) performed a series of wave-tank experiments to evaluate the nonlinear energy transfer from the difference of $\Psi(\omega)$ obtained at various locations along the wavetank. However, the experimental result shows a large scatter from case to case, and we cannot derive any definite conclusion from their work. The most promising approach for this purpose would certainly be numerical experiments. In this paper, we deterministically trace the temporal evolution of random wave fields by integrating numerically the primitive equations for surface gravity waves, and then evaluate the nonlinear energy transfer from the rate of change of the spectrum.

In § 2, we first review the fundamentals such as the primitive governing equations for surface gravity waves, Zakharov's Hamiltonian formalism and the complex amplitude function $b(\boldsymbol{k})$. In § 3, we present the numerical results for the one-dimensional and the two-dimensional transfer functions $T_1(\omega)$ and $T_2(\omega, \theta)$, and compare them with Hasselmann's S_{nl}. Conclusions and discussion are given in § 4.

2. Fundamentals

2.1. *Governing equations*

We consider the irrotational motion of water which is assumed to be inviscid and incompressible. The flow can be described by a velocity potential $\phi(\boldsymbol{x}, z, t)$ which satisfies Laplace's equation within the water. The water depth is assumed to be infinite. Then the governing equations for the motion of nonlinear surface gravity waves are

$$\nabla^2\phi(\boldsymbol{x}, z, t) = 0, \qquad -\infty < z \leqslant \eta(\boldsymbol{x}, t), \tag{2.1}$$

$$\phi_t + gz + \tfrac{1}{2}(\nabla\phi)^2 = 0, \qquad z = \eta(\boldsymbol{x}, t), \tag{2.2}$$

$$\eta_t + \nabla_h\phi \cdot \nabla_h\eta = \phi_z, \qquad z = \eta(\boldsymbol{x}, t), \tag{2.3}$$

$$\phi \to 0, \qquad z \to -\infty, \tag{2.4}$$

where $\eta(\boldsymbol{x}, t)$ is the free surface displacement and $\nabla_h \equiv (\partial/\partial x, \partial/\partial y)$ is the gradient operator in the horizontal (x, y)-plane. The vertical coordinate z is pointing upward with its origin located at the mean free surface. In terms of the velocity potential $\psi(\boldsymbol{x}, t)$ $(= \phi(\boldsymbol{x}, \eta(\boldsymbol{x}, t), t))$ evaluated at the free surface, the boundary conditions (2.2), (2.3) can be rewritten as

$$\psi_t + g\eta + \tfrac{1}{2}(\nabla_h\psi)^2 - \tfrac{1}{2}W^2\left\{1 + (\nabla_h\eta)^2\right\} = 0, \tag{2.5}$$

$$\eta_t + \nabla_h\psi \cdot \nabla_h\eta - W\left\{1 + (\nabla_h\eta)^2\right\} = 0, \tag{2.6}$$

where $W(\boldsymbol{x}, t)$ denotes the vertical velocity evaluated at the free surface.

In order to follow the unsteady evolution of a wave field numerically according to (2.5) and (2.6), we need to solve a Dirichlet problem of Laplace's equation for $\phi(\boldsymbol{x}, z, t)$ to obtain $W(\boldsymbol{x}, t)$ at each time step. For this purpose we employ the high-order spectral method (abbreviated as HOSM hereinafter) developed independently by West *et al.* (1987) and Dommermuth & Yue (1987). A concise review of HOSM can also be found in Tanaka (2001). In this method the wave field is assumed to be periodic in both the x- and y-directions, and the Dirichlet problem for $\phi(\boldsymbol{x}, z, t)$ is solved very efficiently by combining the techniques of amplitude expansion and the fast Fourier transform. Once W is obtained, we can update $\eta(\boldsymbol{x}, t)$ and $\psi(\boldsymbol{x}, t)$ to the next time step by integrating (2.5) and (2.6) numerically by the Runge–Kutta method or some other standard method for ordinary differential equations. Between the two slightly different versions of HOSM, we choose the version by West *et al.* (1987) rather than the one by Dommermuth & Yue (1987) because only the former treats the boundary conditions (2.5), (2.6) in a consistent manner with respect to $\{\eta(\boldsymbol{x}, t), \psi(\boldsymbol{x}, t)\}$, which turn out to be a pair of canonical variables of Zakharov's Hamiltonian formalism of the water wave problem as discussed below.

2.2. *Complex amplitude function* $b(\boldsymbol{k})$

Zakharov (1968) has proved that the boundary value problem specified by (2.1), (2.5), (2.6) can be expressed as a pair of canonical equations

$$\frac{\partial\eta(\boldsymbol{x}, t)}{\partial t} = \frac{\delta H}{\delta\psi(\boldsymbol{x}, t)}, \qquad \frac{\partial\psi(\boldsymbol{x}, t)}{\partial t} = -\frac{\delta H}{\delta\eta(\boldsymbol{x}, t)}, \tag{2.7}$$

by employing the total energy

$$H = \frac{1}{2}\int \mathrm{d}\boldsymbol{x} \int_{-\infty}^{\eta} (\nabla\phi)^2 \,\mathrm{d}z + \frac{g}{2}\int \eta^2 \,\mathrm{d}\boldsymbol{x} \tag{2.8}$$

as the Hamiltonian and $\{\eta(\boldsymbol{x},t),\ \psi(\boldsymbol{x},t)\}$ as the pair of canonical variables. He also introduced a very convenient new canonical variable $b(\boldsymbol{k},t)$, which we call the 'complex amplitude function' here, by

$$b(\boldsymbol{k},t)=\left(\frac{\omega(\boldsymbol{k})}{2k}\right)^{1/2}\hat{\eta}(\boldsymbol{k},t)+\mathrm{i}\left(\frac{k}{2\omega(\boldsymbol{k})}\right)^{1/2}\hat{\psi}(\boldsymbol{k},t),\qquad \omega(\boldsymbol{k})=(gk)^{1/2}, \tag{2.9}$$

where $\hat{\eta}(\boldsymbol{k})$ and $\hat{\psi}(\boldsymbol{k})$ denote, respectively, the Fourier transform of $\eta(\boldsymbol{x})$ and $\psi(\boldsymbol{x})$. In terms of $b(\boldsymbol{k},t)$, the evolution of the wave field can be described by a single complex-valued equation:

$$\mathrm{i}\frac{\partial\, b(\boldsymbol{k},t)}{\partial t}=\frac{\delta H(b,b^*)}{\delta\, b^*(\boldsymbol{k},t)}, \tag{2.10}$$

where the asterisk denotes complex conjugation. In terms of $b(\boldsymbol{k},t)$, variables $\eta(\boldsymbol{x})$ and $\psi(\boldsymbol{x})$ are expressed as

$$\eta(\boldsymbol{x})=\frac{1}{2\pi}\int\left(\frac{k}{2\omega(\boldsymbol{k})}\right)^{1/2}\{b(\boldsymbol{k})+b^*(-\boldsymbol{k})\}\,\mathrm{e}^{\mathrm{i}\boldsymbol{k}\cdot\boldsymbol{x}}\,\mathrm{d}\boldsymbol{k}, \tag{2.11}$$

$$\psi(\boldsymbol{x})=\frac{-\mathrm{i}}{2\pi}\int\left(\frac{\omega(\boldsymbol{k})}{2k}\right)^{1/2}\{b(\boldsymbol{k})-b^*(-\boldsymbol{k})\}\,\mathrm{e}^{\mathrm{i}\boldsymbol{k}\cdot\boldsymbol{x}}\,\mathrm{d}\boldsymbol{k}. \tag{2.12}$$

Substituting (2.11), (2.12) into (2.8) and performing the integrals with respect to $\boldsymbol{x}$ and z, we obtain the expressions for the potential energy P_2 (the second term of (2.8)) and the leading-order part K_2 of the kinetic energy (the first term of (2.8)) as follows:

$$P_2=\frac{g}{2}\iint\left(\frac{k}{2\omega(\boldsymbol{k})}\right)\{b(\boldsymbol{k})+b^*(-\boldsymbol{k})\}\{b(-\boldsymbol{k})+b^*(\boldsymbol{k})\}\,\mathrm{d}\boldsymbol{k}, \tag{2.13}$$

$$K_2=-\iint\left(\frac{\omega(\boldsymbol{k})}{4}\right)\{b(\boldsymbol{k})-b^*(-\boldsymbol{k})\}\{b(-\boldsymbol{k})-b^*(\boldsymbol{k})\}\,\mathrm{d}\boldsymbol{k}. \tag{2.14}$$

The sum of these two contributions gives the expression for H_2, the lowest-order part of H, as

$$H_2=\int\omega(\boldsymbol{k})b(\boldsymbol{k})b^*(\boldsymbol{k})\mathrm{d}\boldsymbol{k}, \tag{2.15}$$

which in turn gives the canonical equation for linear waves:

$$\mathrm{i}\frac{\partial b(\boldsymbol{k},t)}{\partial t}=\omega(\boldsymbol{k})b(\boldsymbol{k},t). \tag{2.16}$$

In this respect, $b(\boldsymbol{k})$ plays the role of the normal mode of the linear wave field. The significance of $b(\boldsymbol{k})$ for our present purpose becomes clearer by considering a special case in which $b(\boldsymbol{k})$ is given by a delta function as

$$b(\boldsymbol{k},t)=b_0\delta(\boldsymbol{k}-\boldsymbol{k}_0)\mathrm{e}^{-\mathrm{i}\omega_0 t},\quad \omega_0=\omega(\boldsymbol{k}_0),\quad b_0 \text{ constant}. \tag{2.17}$$

Equations (2.11) and (2.12) then give

$$\eta(\boldsymbol{x},t)=a_0\cos(\boldsymbol{k}_0\cdot\boldsymbol{x}-\omega_0 t+\alpha),\quad \psi(\boldsymbol{x},t)=\left(\frac{\omega_0}{k_0}\right)a_0\sin(\boldsymbol{k}_0\cdot\boldsymbol{x}-\omega_0 t+\alpha), \tag{2.18}$$

where

$$a_0=\frac{1}{\pi}\left(\frac{k_0}{2\omega_0}\right)^{1/2}|b_0|,\qquad \alpha=\arg b_0. \tag{2.19}$$

This demonstrates that, when the wave field is described in terms of a distribution of $b(\boldsymbol{k})$ on the $\boldsymbol{k}$-plane, each point, $\boldsymbol{k}_0$ say, on the $\boldsymbol{k}$-plane corresponds to a uniform wavetrain of progressive surface gravity waves with wavenumber $\boldsymbol{k}_0$, and its amplitude and the phase constant are determined by $b(\boldsymbol{k}_0)$.

As explained before, we trace the evolution of a wave field by integrating (2.5) and (2.6) numerically. Therefore the raw data which we get directly from the numerical computation at each time step are $\eta(\boldsymbol{x}, t)$ and $\psi(\boldsymbol{x}, t)$. On the other hand, what we want is a spectrum like $\Phi(\omega, \theta, t)$, and to estimate it we need to interpret the wave field as a superposition of component waves. The above result implies that this changeover from the description of the wave field in terms of $\{\eta(\boldsymbol{x}), \psi(\boldsymbol{x})\}$ to the one in terms of the spectrum $\Phi(\omega, \theta)$ can be achieved quite easily by making use of $b(\boldsymbol{k})$.

2.3. *Relation between $b(\boldsymbol{k})$ and $\Phi(\omega, \theta)$*

In our implementation of HOSM the wave field is assumed to be periodic both in x and y with period L_x and L_y, respectively. Hence the wavenumber vector $\boldsymbol{k}$ is discretized as

$$\boldsymbol{k} = (k_x, k_y) = \left(\frac{2\pi k}{L_x}, \frac{2\pi l}{L_y}\right) \qquad (k, l \text{ integer}). \tag{2.20}$$

Then $\eta(\boldsymbol{x})$ and $\psi(\boldsymbol{x})$ are represented by discrete Fourier transforms as

$$\eta(\boldsymbol{x}) = \sum_{\boldsymbol{k}} \hat{\eta}_{\boldsymbol{k}} \mathrm{e}^{\mathrm{i}\boldsymbol{k}\cdot\boldsymbol{x}}, \quad \psi(\boldsymbol{x}) = \sum_{\boldsymbol{k}} \hat{\psi}_{\boldsymbol{k}} \mathrm{e}^{\mathrm{i}\boldsymbol{k}\cdot\boldsymbol{x}}, \tag{2.21}$$

and $b(\boldsymbol{k})$ is given correspondingly by

$$b_{\boldsymbol{k}} = \left(\frac{\omega_{\boldsymbol{k}}}{2|\boldsymbol{k}|}\right)^{1/2} \hat{\eta}_{\boldsymbol{k}} + \mathrm{i}\left(\frac{|\boldsymbol{k}|}{2\omega_{\boldsymbol{k}}}\right)^{1/2} \hat{\psi}_{\boldsymbol{k}}, \qquad \omega_{\boldsymbol{k}} = \omega(\boldsymbol{k}). \tag{2.22}$$

Each mesh point on the $\boldsymbol{k}$-plane represents a component wave with corresponding wavenumber as discussed above.

The energy density E is given by

$$E = \frac{1}{A}\left[\frac{1}{2}\int_A \mathrm{d}\boldsymbol{x} \int_{-\infty}^{\eta} (\nabla\phi)^2 \,\mathrm{d}z + \frac{g}{2}\int_A \eta^2 \,\mathrm{d}\boldsymbol{x}\right], \tag{2.23}$$

where A denotes the rectangle $0 \leqslant x \leqslant L_x$, $0 \leqslant y \leqslant L_y$ on the $\boldsymbol{x}$-plane. Substituting the relations

$$\hat{\eta}_{\boldsymbol{k}} = \left(\frac{|\boldsymbol{k}|}{2\omega_{\boldsymbol{k}}}\right)^{1/2} \left(b_{\boldsymbol{k}} + b^*_{-\boldsymbol{k}}\right), \quad \hat{\psi}_{\boldsymbol{k}} = -\mathrm{i}\left(\frac{\omega_{\boldsymbol{k}}}{2|\boldsymbol{k}|}\right)^{1/2} \left(b_{\boldsymbol{k}} - b^*_{-\boldsymbol{k}}\right) \tag{2.24}$$

into (2.23) and performing the integrals with respect to $\boldsymbol{x}$ and z, we obtain the leading-order approximation for E in terms of $b_{\boldsymbol{k}}$ as follows:

$$E \approx \sum_{\boldsymbol{k}} \omega_{\boldsymbol{k}} |b_{\boldsymbol{k}}|^2. \tag{2.25}$$

On the other hand, E can also be expressed by the directional spectrum $\Phi(\omega, \theta)$ as

$$E = \int_0^{2\pi}\int_0^{\infty} \Phi(\omega, \theta)\,\mathrm{d}\omega\,\mathrm{d}\theta = \int \frac{g^2}{2\omega(\boldsymbol{k})^3}\Phi(\omega, \theta)\mathrm{d}\boldsymbol{k} \approx \sum_{\boldsymbol{k}} \frac{g^2}{2\omega_{\boldsymbol{k}}^3}\Phi(\omega, \theta)\Delta S_{\boldsymbol{k}}, \tag{2.26}$$

where $\Delta S_{\boldsymbol{k}}$ is the area of a rectangular mesh on the $\boldsymbol{k}$-plane given by

$$\Delta S_{\boldsymbol{k}} = \Delta k_x \times \Delta k_y = \left(\frac{2\pi}{L_x}\right) \times \left(\frac{2\pi}{L_y}\right). \tag{2.27}$$

Equating (2.25) and (2.26) gives an approximate relation between $|b_{\boldsymbol{k}}|$ and $\Phi(\omega,\theta)$ as follows:

$$|b_{\boldsymbol{k}}|^2 \approx \frac{g^2}{2\omega_{\boldsymbol{k}}^4}\Phi(\omega,\theta)\Delta S_{\boldsymbol{k}}. \tag{2.28}$$

This relation enables us to construct a distribution of $\{b_{\boldsymbol{k}}\}$ when the energy spectrum of the wave field is prescribed. The initial phases of $\{b_{\boldsymbol{k}}\}$ are given by a homogeneous random number in $[0, 2\pi]$.

We assume that $\Phi(\omega,\theta)$ is expressed as $\Phi(\omega,\theta) = \Psi(\omega)G(\theta)$ with

$$\Psi(\omega) = \alpha g^2\omega^{-5}\exp\left[-\frac{5}{4}\left(\frac{\omega}{\omega_p}\right)^{-4}\right]\gamma^{\exp[-(\omega-\omega_p)^2/(2\sigma^2\omega_p^2)]}, \tag{2.29}$$

and

$$G(\theta) = \begin{cases} (2/\pi)\cos^2\theta, & |\theta| \leqslant \pi/2 \\ 0, & |\theta| > \pi/2, \end{cases} \tag{2.30}$$

where α is a non-dimensional coefficient called the Phillips constant, and ω_p is the angular frequency at the peak of the spectrum. From now on, we employ the normalization of space and time such that both ω_p and g are unity. Under this normalization, the frequency spectrum $\Psi(\omega)$ is written as

$$\Psi(\omega) = \alpha\,\omega^{-5}\exp\left(-\frac{5}{4\omega^4}\right)\gamma^{\exp[-(\omega-1)^2/2\sigma^2]}. \tag{2.31}$$

In the following, we call $\Phi(\omega,\theta)$ the JONSWAP spectrum when

$$\alpha = 3.279E, \qquad \gamma = 3.3, \qquad \sigma = \begin{cases} 0.07 & (\omega < 1) \\ 0.09 & (\omega \geqslant 1), \end{cases} \tag{2.32}$$

and the Pierson–Moskowitz(P-M) spectrum when

$$\alpha = 5E, \qquad \gamma = 1.0. \tag{2.33}$$

The relations between α and E in (2.32) and (2.33) have come from the fact that

$$\int_0^\infty \omega^{-5}\exp\left(-\frac{5}{4\omega^4}\right)\gamma^{\exp[-(\omega-1)^2/2\sigma^2]}\,\mathrm{d}\omega = \begin{cases} 1/3.279 & \text{if } \gamma = 3.3 \\ 1/5 & \text{if } \gamma = 1.0. \end{cases} \tag{2.34}$$

3. Numerical results

3.1. *Parameters*

We follow the temporal evolution of wave fields according to the free surface boundary conditions (2.5) and (2.6). The vertical velocity $W(\boldsymbol{x},t)$ is evaluated by HOSM, and the integration in time is performed by the fourth-order Runge–Kutta method. In the integration in time, we update $\{b_{\boldsymbol{k}}\mathrm{e}^{\mathrm{i}\omega_{\boldsymbol{k}}t}\}$ instead of $\{b_{\boldsymbol{k}}(t)\}$ or $\{\eta(\boldsymbol{x},t),\psi(\boldsymbol{x},t)\}$ because this enables us to use a larger step size Δt without losing numerical accuracy (Tanaka 2001).

The numbers of mesh points (N_x, N_y) in the physical space $(x,y$-plane) and the order of nonlinearity M are fixed, respectively, as $N_x = 2^{12} = 4096$, $N_y = N_x/2 = 2048$ and $M = 3$ in all the computations discussed below. The x-axis is taken along the principal direction of propagation. The choice $M = 3$ implies that we take account all of the three-wave and four-wave nonlinear interactions, irrespective of whether

resonant or non-resonant. Considering the condition for the numerical computation to be free from aliasing errors, the maximum mode numbers $k_{\max}$ in the x-direction and $l_{\max}$ in the y-direction are determined, respectively, as $k_{\max} = N_x/(M+1) = 1024$ and $l_{\max} = N_y/(M+1) = 512$. Note that k, l, $k_{\max}$ and $l_{\max}$, as well as k_p appearing below, denote mode numbers and hence are integers, while k_x and k_y are components of vector wavenumbers and take real values.

The relation between (N_x, N_y) and $(k_{\max}, l_{\max})$ employed above may need explanation. Let $k_{\max}$ be the mode number corresponding to the largest wavenumber that we want to describe correctly, and N_x be the number of mesh points in the physical space. Suppose that the order of nonlinearity is M and the prescribed wave field consists of those waves with mode numbers up to $k_{\max}$. Then the nonlinearity in the boundary conditions would generate wave modes up to $Mk_{\max}$, and aliasing error occurs if $Mk_{\max} > N_x/2$. However the aliasing error affects only those modes with mode number k which satisfy

$$k > \tfrac{1}{2}N_x - (Mk_{\max} - \tfrac{1}{2}N_x) = N_x - Mk_{\max}, \tag{3.1}$$

and those modes with k less than $k_{\max}$ would evade the contamination by aliasing error if we take N_x large enough to satisfy the condition

$$k_{\max} < N_x - Mk_{\max}, \qquad \text{i.e.} \qquad N_x > (M+1)k_{\max}. \tag{3.2}$$

This is the method of aliasing removal which West *et al.* (1987) employed, and we follow them in this paper. When $M = 2$, this method reduces to the well-known '3/2-rule' which is often used in computational fluid dynamics (e.g. Canuto *et al.* 1988).

When the θ-dependence of $\Phi(\omega, \theta)$ is proportional to $\cos^2\theta$ as assumed here, the ratio $\bar{k}_x/\bar{k}_y$ of the average wavenumbers is defined by

$$\bar{k}_x/\bar{k}_y = \int k_x \epsilon(\boldsymbol{k})\,\mathrm{d}\boldsymbol{k} \Big/ \int k_y \epsilon(\boldsymbol{k})\,\mathrm{d}\boldsymbol{k} = 2. \tag{3.3}$$

Accordingly it would be reasonable to fix the large-wavenumber cutoff of k_x to be twice that of k_y, and this explains why we use twice the number of points in the x-direction than in the y-direction. As the mode numbers k and l vary in the range $-k_{\max} \leqslant k \leqslant k_{\max}$ and $-l_{\max} \leqslant l \leqslant l_{\max}$, the total number of component waves whose temporal evolution we are to follow amounts to more than 2 million (2049×1025, more precisely).

In most computations, we require that the maximum mode number $k_{\max}$ corresponds to the 15th harmonic of the peak of the spectrum. This fixes the mode number k_p of the peak as $k_p = k_{\max}/15 = 68$, implying that the region on the physical $\boldsymbol{x}$-plane which is treated by the numerical computation is a square with area $68\lambda_p \times 68\lambda_p$, with $\lambda_p (= 2\pi)$ being the wavelength corresponding to the peak of the spectrum. On the other hand, the corresponding region on the $\boldsymbol{k}$-plane is a rectangle $-15 \leqslant k_x \leqslant 15$, $-7.5 \leqslant k_y \leqslant 7.5$, and it is covered by a uniform square mesh with a mesh size $1/68 \times 1/68$. The wavenumber cut off at $15k_p$ in k_x and $7.5k_p$ in k_y may appear needlessly high, but this turns out not to be sufficient, at least for the case with the P-M spectrum, as we discuss in § 3.4 below.

The energy density E is varied in the range $0.002 \leqslant E \leqslant 0.005$, and the corresponding range of the significant waveheight $H_{1/3}$ is $0.179 \leqslant H_{1/3} \leqslant 0.283$ if estimated by the relation $H_{1/3} \approx 4\sqrt{E}$. Note that this is the range of $H_{1/3}$ when the dominant wavelength is normalized to 2π. If the peak frequency is 1/8 Hz and

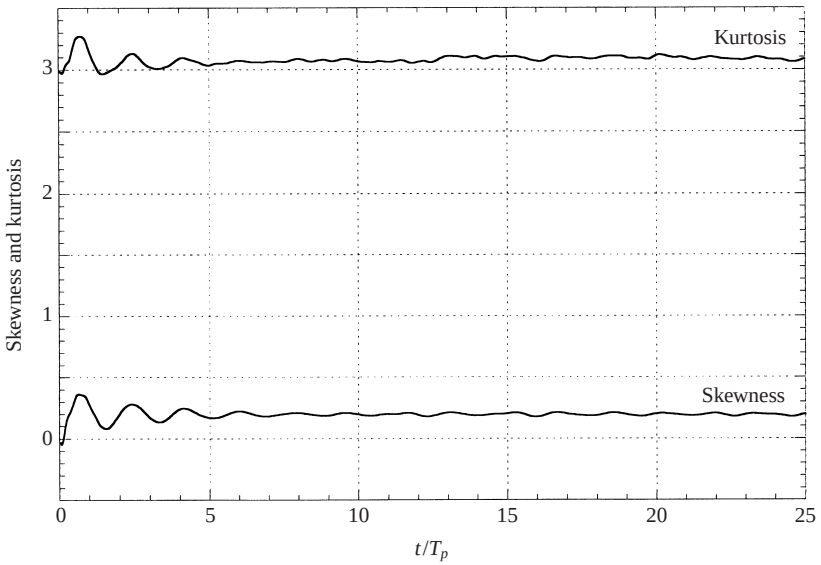

FIGURE 1. Evolution of skewness S and kurtosis K of $\eta(\boldsymbol{x}, t)$: case[E005J_1].

hence the dominant wavelength is 100 m, the range of $H_{1/3}$ as above corresponds to $2.85\,\mathrm{m} \leqslant H_{1/3} \leqslant 4.50\,\mathrm{m}$.

The step size Δt of time integration is fixed as $T_p/25$, with T_p being the period corresponding to the peak of the spectrum, and is 2π according to our normalization. The duration of computation is $20T_p$ for most of the computations, while it is extended to $30T_p$ for some special cases. The accuracy of the computation is checked by monitoring the variation of the total energy

$$E_{\mathrm{total}} = \frac{1}{2}\iint \psi \frac{\partial \eta}{\partial t}\,\mathrm{d}\boldsymbol{x} + \frac{1}{2}\iint \eta^2\,\mathrm{d}\boldsymbol{x}, \tag{3.4}$$

which is an integral of motion of the system. Although the accuracy varies from case to case, E_{total} remains constant within about 1% throughout most of the computations.

In the following we use a simple notation to specify each of the computations. For example, case[E005J_3] denotes the third run of a series of computations in which the initial spectrum is given by the JONSWAP spectrum (2.31) with $E = 0.005$.

3.2. *Statistics of* $\eta(\boldsymbol{x}, t)$

Figure 1 shows the evolution of the skewness S and the kurtosis K of $\eta(\boldsymbol{x}, t)$ obtained from the case[E005J_1] which are defined respectively by

$$S = \frac{1}{N_x N_y}\sum_{i=1}^{N_x}\sum_{j=1}^{N_y} \eta_{i,j}^3 \Big/ \eta_{\mathrm{rms}}^3, \qquad K = \frac{1}{N_x N_y}\sum_{i=1}^{N_x}\sum_{j=1}^{N_y} \eta_{i,j}^4 \Big/ \eta_{\mathrm{rms}}^4, \tag{3.5}$$

where $\eta_{i,j}$ is the value of $\eta(\boldsymbol{x}, t)$ at the (i, j) grid point on the (x, y)-plane. It can be observed that both S and K fluctuate around some mean values which are slightly larger than those corresponding to the Gaussian distribution (i.e. $S = 0$, $K = 3$). The figure also suggests the existence of a transient process during the first few periods.

As explained in § 2, the initial wave field is constructed as a superposition of sinusoidal wavetrains, i.e. the solutions of the linearized system. When this artificially created wave field is left to evolve according to the governing equations for nonlinear

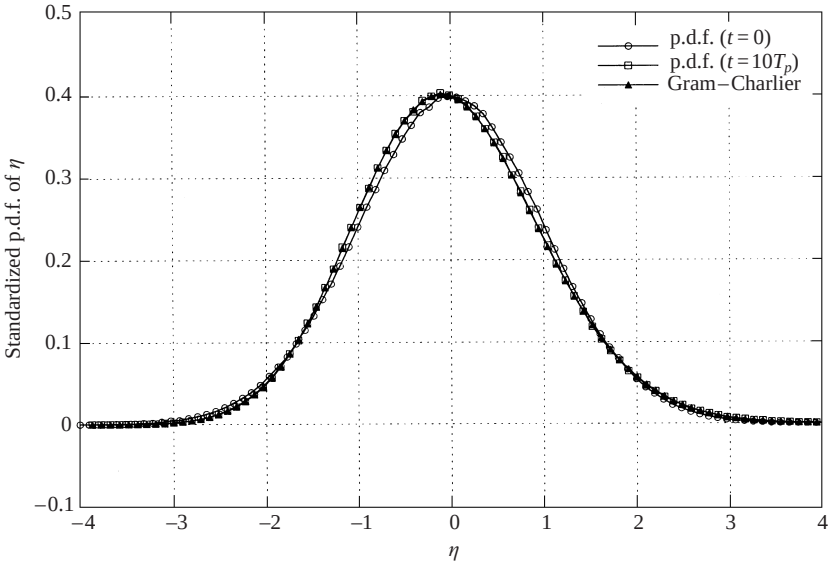

FIGURE 2. Comparison of standardized p.d.f. of η and the third-order Gram–Charlier Series: case[E005J_1].

water waves, the nonlinear interactions among component waves generate bound waves at the sums and the differences of their wavenumber vectors. This generation of bound waves or harmonics results in the fluctuations of S and K shown in figure 1. During this process of transition, the three-wave interactions appear to dominate over other nonlinear interactions because they are of lowest order, hence most effective, in such a short time as a few periods. This view is also supported by the period of oscillation of S and K, observed in figure 1 to be about 1.7. This can be identified as the period of the beat between the bound waves at $2\boldsymbol{k}_p$ with frequency $2\omega(\boldsymbol{k}_p)$ $(= 2)$, which is generated by the three-wave interaction $\boldsymbol{k}_p + \boldsymbol{k}_p = 2\boldsymbol{k}_p$, and the free wave at $2\boldsymbol{k}_p$ whose frequency is $\omega(2\boldsymbol{k}_p) = \sqrt{2}$.

The large fluctuations of S and K almost disappear by $t \approx 5T_p$, and they remain nearly constant afterwards. This fact suggests that the initial wave field, which is just a superposition of linear free waves, has transformed to a 'consistent' nonlinear wave field during the first few periods. By a 'consistent' nonlinear wave field, we mean a wave field in which the free wave components accompany the corresponding bound waves which they are supposed to accompany, just like the bound wave $(1/2)a^2k\cos 2(kx - \omega t)$ for the free wave $a\cos(kx - \omega t)$ in a Stokes wave. In the evaluation of the nonlinear energy transfer which is discussed below, we will discard the data obtained from the interval $0 \leqslant t \leqslant 6T_p$. Although we have not employed it here, the initialization procedure developed by Dommermuth (2000) might be able to generate more appropriate initial wave fields.

Figure 2 shows the probability density function (p.d.f.) of $\eta(\boldsymbol{x}, t)$ obtained from case[E005J_1] at $t = 0$ and $t = 10T_p$. The p.d.f. has been standardized such that the mean is 0 and the standard deviation is 1. In the same figure is also shown the third-order Gram–Charlier series with the same skewness as η at $t = 10T_p$, which fits perfectly well to the standardized p.d.f. of η at that time. For standardization and the Gram–Charlier distribution, see Stuart & Ord (1994). The p.d.f. at $t = 0$ is nearly Gaussian as being expected from its method of construction, and differs significantly

from that evaluated at $t = 10T_p$. On the other hand, the p.d.f. at $t = 20T_p$, although not shown here, is almost the same as that evaluated at $t = 10T_p$. This fact supports our supposition that a 'consistent' and quasi-steady nonlinear wave field has been built up by $t = 10T_p$.

3.3. *Frequency spectrum* $\Psi(\omega)$

As explained in § 2, the energy density E is given approximately in terms of $\{b_{\boldsymbol{k}}\}$ by

$$E \approx \sum_{\boldsymbol{k}} \omega_{\boldsymbol{k}} |b_{\boldsymbol{k}}|^2 = \sum_{k,l} \omega_{k,l} |b_{k,l}|^2. \tag{3.6}$$

On the other hand, it is also given, by definition, in terms of the frequency spectrum $\Psi(\omega)$ by

$$E = \int_0^\infty \Psi(\omega)\, \mathrm{d}\omega \approx \sum_j \Psi(j\Delta\omega)\Delta\omega. \tag{3.7}$$

Combining these two equations, we obtain an approximate expression for $\Psi(\omega)$ at discrete values of ω with an interval $\Delta\omega$ as follows:

$$\Psi(j\Delta\omega) \approx \sum_{k,l}{}' \omega_{k,l} |b_{k,l}|^2 \Big/ \Delta\omega \qquad (j = 1, 2, \ldots), \tag{3.8}$$

where $\sum'_{k,l}$ denotes summation over those pairs of mode numbers (k, l) that satisfy the condition

$$(j - \tfrac{1}{2})\Delta\omega \leqslant \omega_{k,l} < (j + \tfrac{1}{2})\Delta\omega. \tag{3.9}$$

The choice of the frequency resolution $\Delta\omega$ is rather subtle. Use of too large $\Delta\omega$ would blur the fine structure of the true spectrum, while too small $\Delta\omega$ would give a jagged spectrum due to insufficient smoothing. Here we fix $\Delta\omega$ as $1/20$ (remember that $\omega_p = 1$). An interval $[\omega - \Delta\omega/2, \omega + \Delta\omega/2]$ on the ω-axis corresponds to a circular ring on the $\boldsymbol{k}$-plane with radius ω^2 and width $2\omega\Delta\omega$. Because the area of the ring is $4\pi\omega^3\Delta\omega$ and the area of one mesh on the $\boldsymbol{k}$-plane is $1/k_p^2$, the number of component waves, which is equal to the number of mesh points, that will fall in the interval $[\omega - \Delta\omega/2, \omega + \Delta\omega/2]$ is given by $4\pi\omega^3\Delta\omega\, {k_p}^2$. When $k_p = 68$ and $\Delta\omega = 1/20$, the single marker point at $\omega = 1$ on a graph of $\Psi(\omega)$ like that shown in figure 3 below represents some 2900 component waves, while the marker point at $\omega = 2$ represents more than 23 000 component waves.

Figure 3 shows $\Psi(\omega)$ which is obtained in this way for the case[E005J_1] at $t = 10T_p$ and $t = 25T_p$. It should be noted that $\Psi(\omega)$ evolves in time quite slowly, and remains almost the same during such a short interval as $15T_p$. According to Hasselmann's theory, the nonlinear energy transfer S_{nl}, which also gives the rate of change of $\Psi(\omega)$ as indicated by (1.5), is of $O(E^3)$ while the magnitude of $\Psi(\omega)$ itself is $O(E)$, hence the characteristic time scale of the evolution of $\Psi(\omega)$ is of $O(E^{-2})$. This implies that it would take at least several thousands of periods for $\Psi(\omega)$ to experience an appreciable change when $E = O(10^{-3})$, typical of real oceans. (Remember also that the range of E we consider here is $0.002 \leqslant E \leqslant 0.005$.) The purpose of this work is to evaluate the energy transfer from such a slight change of $\Psi(\omega, t)$ as shown in figure 3. Thus the success of this attempt obviously depends on the accurate estimate of $\Psi(\omega)$.

As described in § 3.1, we trace the evolution of more than two million component waves. The reason for treating so many is to increase the accuracy of the estimated spectrum. According to the theory of spectral estimate (see, for example, Newland

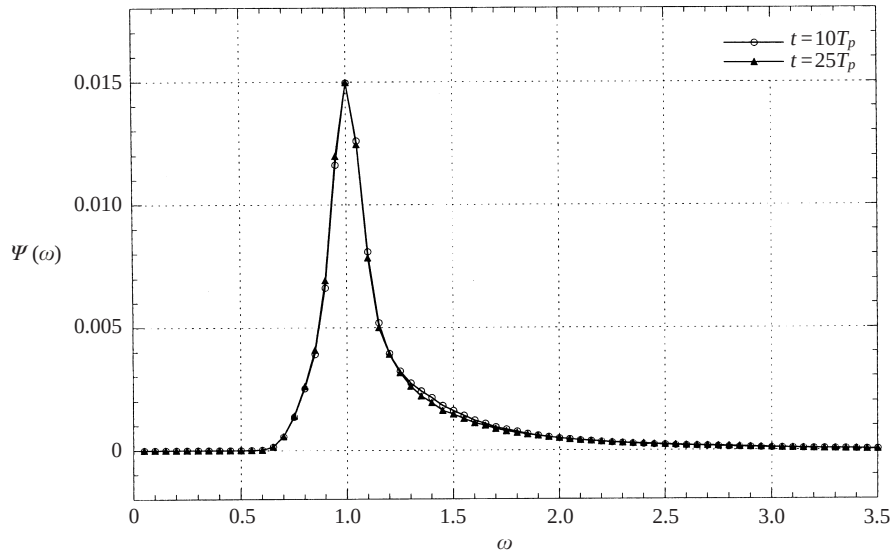

FIGURE 3. Frequency spectrum $\Psi(\omega)$ obtained at $t = 10T_p$ and $25T_p$: case[E005J_1].

1993 and Bendat & Piersol 1986), the variance of the estimated spectrum decreases inversely proportional to the statistical degrees of freedom, which is given, in our case, by twice the number of component waves which will fall into a single bin of width $\Delta\omega$. As this is proportional to k_p^2 as discussed above, we need to use a sufficiently fine mesh on the $\boldsymbol{k}$-plane to make the statistical degrees of freedom, and hence the reliability of the estimated spectrum, large enough. At the same time, the $\boldsymbol{k}$-plane should also be wide enough if we are to include sufficiently higher harmonics such as the fifteenth harmonic of the peak mode. In order to fulfil both these requirements simultaneously, use of such a huge number of component waves as two million is inevitable so long as we are to describe the wave field based on Fourier-series representation.

Further, there is another reason to use a very fine mesh on the $\boldsymbol{k}$-plane. As Kartashova (1998) discusses, the evolution of a discrete system can be essentially different from that of a continuous system. So we should be careful not to allow the discreteness of the numerical simulation to affect the result in any serious manner. It should be stressed that the sparsity of the mesh on the $\boldsymbol{k}$-plane can never be compensated for, however many realizations we may use in the estimate of the spectrum by their arithmetic mean. On the contrary, the number of realizations necessary for obtaining a statistically reliable result can be very small, provided the numerical domain on the $\boldsymbol{k}$-plane is wide enough and, at the same time, discretized finely enough as we will show below.

3.4. *One-dimensional transfer* $T_1(\omega)$

We have employed two methods for estimating the one-dimensional nonlinear energy transfer $T_1(\omega)$. In the first and simpler method, $T_1(\omega)$ is estimated by dividing the difference between $\Psi(\omega, t)$ evaluated at two different times, t_1 and t_2 say, by the interval $t_2 - t_1$:

$$T_1(\omega) = \frac{\Psi(\omega, t_2) - \Psi(\omega, t_1)}{t_2 - t_1}. \tag{3.10}$$

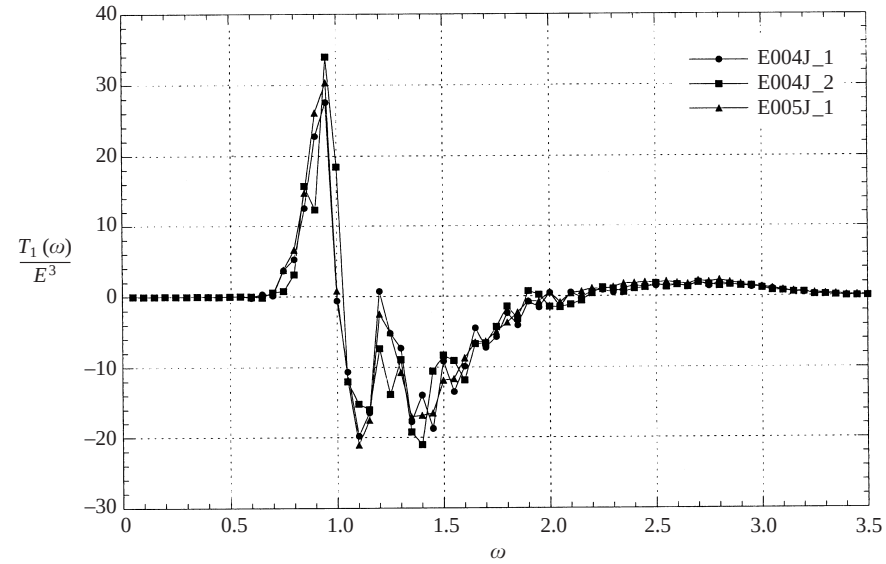

FIGURE 4. $T_1(\omega)/E^3$ estimated by the first method for the JONSWAP spectrum.

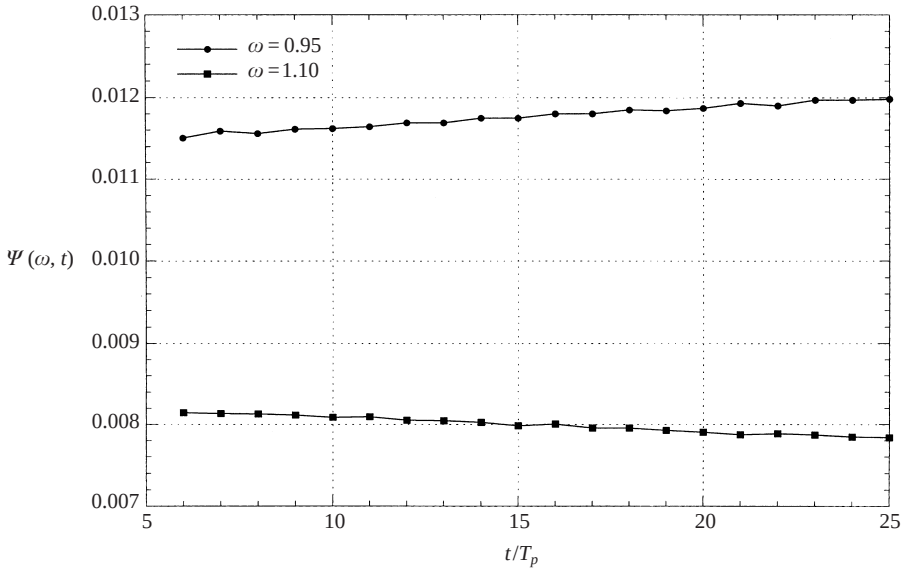

FIGURE 5. $\Psi(0.95)$ and $\Psi(1.10)$ as functions of t/T_p: case[E005J_1].

Figure 4 shows $T_1(\omega)$ thus obtained for three cases with the JONSWAP spectrum: cases[E004J_1], [E004J_2] and [E005J_1]. In these estimates of $T_1(\omega)$, t_1 and t_2 are tentatively chosen as $t_1 = 10T_p$ and $t_2 = 25T_p$. The cases[E004J_1] and [E004J_2] have the same E but different distributions of initial phases of the component waves. On the other hand, cases[E004J_1] and [E005J_1] have different E but the distributions of initial phases are the same. Therefore these two cases have exactly the same initial surface profile $\eta(\boldsymbol{x}, 0)$ and the velocity potential $\psi(\boldsymbol{x}, 0)$ when scaled by $\sqrt{E}$. Of course, this proportionality is lost immediately once the system starts to evolve according to the nonlinear evolution equations (2.5) and (2.6). Hasselmann's

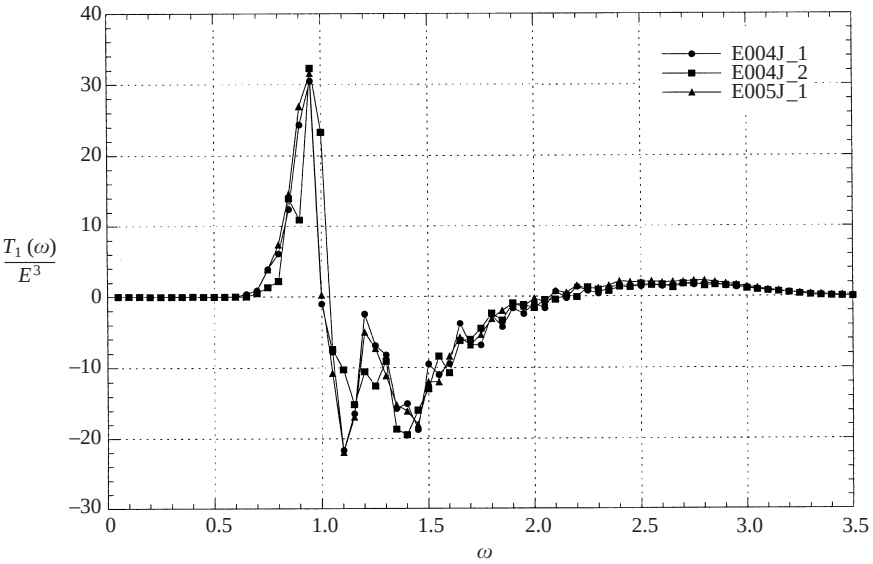

FIGURE 6. $T_1(\omega)/E^3$ estimated by the second method for the JONSWAP spectrum.

theory predicts that the nonlinear energy transfer is proportional to E^3 as depicted in (1.4), and in figure 4 we show $T_1(\omega)/E^3$ to facilitate the comparison between cases with different values of E.

The second method for estimating $T_1(\omega)$ is based on the evolution of $\Psi(\omega)$ in t at fixed values of ω. Figure 5 shows $\Psi(\omega, t)$ for $\omega = 0.95$ and 1.10 as functions of t which are obtained from case[E005J_1]. It can be observed that, for both values of ω, $\Psi(\omega, t)$ changes almost linearly in t, implying that $T_1(\omega)$ remains nearly constant during that period. Actually, when we fit a straight line to each of the curves shown in the figure by the least-square method, the correlation coefficient is about 0.99 for both curves. The slope of the best-fit straight line gives an estimate for $T_1(\omega)$. In doing this we have discarded the data from the first six periods by considering the initial transient process discussed in § 3.2. Figure 6 shows $T_1(\omega)$ estimated by this second method for the same cases as those shown in figure 4. In this second method, the $\Psi(\omega)$ at all output time steps are utilized, and hence we can expect to obtain better results. Actually $T_1(\omega)$ obtained by the second method shows a smaller dispersion among cases than that obtained by the first method, particularly around the peak of the spectrum. From now on we will estimate $T_1(\omega)$ only by the second method by using $\Psi(\omega, t)$ between $6T_p < t \leqslant 20T_p$.

3.4.1. *JONSWAP spectrum*

In figure 7 we show $T_1(\omega)$ obtained from sixteen runs all of which have the JONSWAP spectrum with $E = 0.004$ at $t = 0$. They differ only in the distribution of initial phases of the component waves. The figure gives a rough estimate of the variability of $T_1(\omega)$ from run to run. The difference between runs is very small for the high-frequency region where $\omega \geqslant 2\omega_p$. As discussed in § 3.3, the reliability of our estimate of $\Psi(\omega)$ increases in proportion to ω^3. The result shown in figure 7 strongly suggests that we would be able to obtain an estimate for $T_1(\omega)$, whose scatter is very small and is hence quite reliable not only in the high-frequency region but also in the region around the peak of the spectrum, if the numerical mesh on the $\boldsymbol{k}$-plane is 2^3

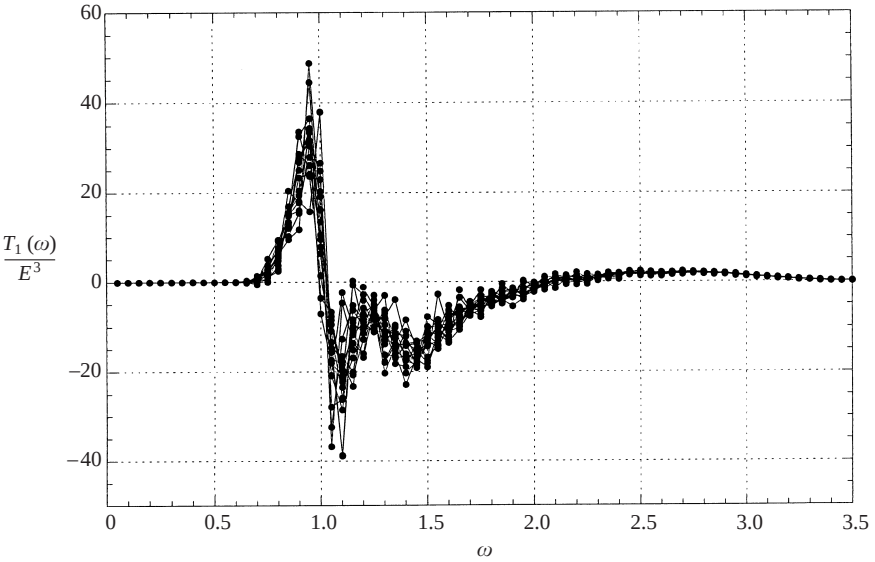

FIGURE 7. $T_1(\omega)/E^3$ obtained from 16 runs with the JONSWAP spectrum: $E = 0.004$.

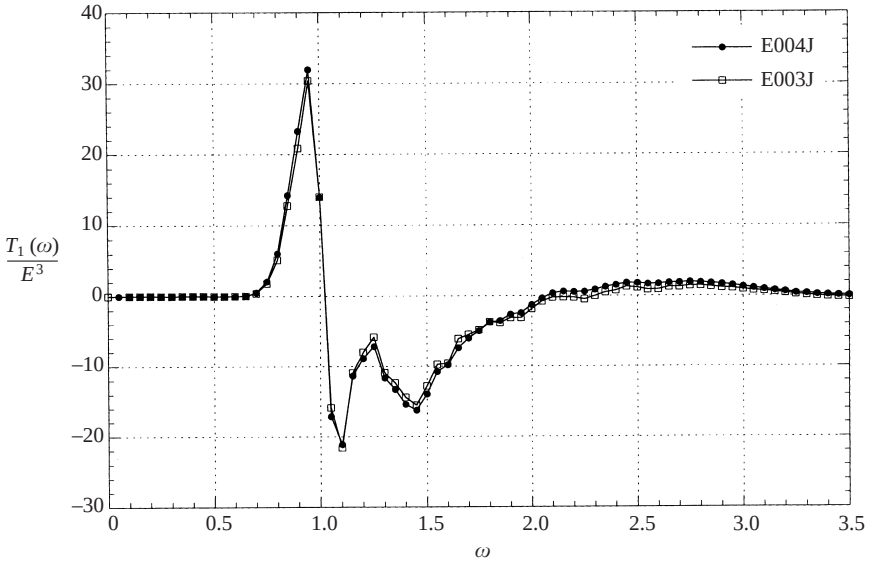

FIGURE 8. Average $T_1(\omega)/E^3$ for the JONSWAP spectrum, $E = 0.003$ and 0.004.

times finer than the present one. Unfortunately, however, computations of this size are not possible for us at the moment.

Figure 8 is the average of sixteen $T_1(\omega)$ shown in figure 7. The corresponding result for $E = 0.003$ is also shown in the figure. The mth run ($m = 1, \ldots, 16$) with $E = 0.003$ and the mth run with $E = 0.004$ have the same distribution of the initial phases. According to (2.32), $E = 0.003$ and $E = 0.004$ correspond to the Phillips constant $\alpha = 0.0098$ and 0.0131 respectively.

In our numerical simulations, all the nonlinear interactions up to four-wave processes are taken into account, irrespective of whether resonant or non-resonant.

Therefore it is not trivial at all that $T_1(\omega)$ can be scaled by E^3. As shown in figure 8, however, $T_1(\omega)$ obtained for two different values of E are almost indistinguishable when divided by E^3. This implies that the lower-order, and hence larger in magnitude, three-wave non-resonant interactions do not affect the evolution of the frequency spectrum $\Psi(\omega)$, as Hasselmann's theory predicts, even for such a short-term evolution as that for $20T_p$. There have been many previous works such as Masuda (1980), Hasselmann & Hasselmann (1981), Resio & Perrie (1991) and Komatsu & Masuda (1996) which have evaluated the analytical expression for $T_1(\omega)$ given by Hasselmann (1962). However, as far as we are aware, this is the first time that $T_1(\omega)$ has been obtained without relying on Hasselmann's theory.

In the following comparison with Hasselmann's theory, $S_{nl}(\omega)$ denotes the one-dimensional nonlinear energy transfer given by Hasselmann's theory, while $T_1(\omega)$ denotes the same quantity but obtained by our direct numerical simulations. Among many previous works which have evaluated $S_{nl}(\omega)$ for the JONSWAP and the P-M spectra with the same θ-dependence as that assumed here, we will compare our result mainly with those of Resio & Perrie (1991), which is abbreviated as RP91 hereinafter. When $\Psi(\omega)$ is the JONSWAP spectrum, the important characteristics of $S_{nl}(\omega)$ as evaluated by previous authors can be summarized as follows: (i) it has a maximum at $\omega \approx 0.95$ and minimum at $\omega \approx 1.1$; (ii) it shows a large oscillation on the high-frequency side of the minimum before becoming positive again at $\omega \approx 2$; (iii) it reaches a positive local maximum at around 2.5, then monotonically diminishes to zero as ω increases further. It can be clearly observed in figure 8 that our $T_1(\omega)$ also possesses all of these characteristics. Thus, as far as the overall pattern is concerned, it would be fair to say that our $T_1(\omega)$ is very close to Hasselmann's $S_{nl}(\omega)$.

Now let us compare $T_1(\omega)$ and $S_{nl}(\omega)$ more quantitatively. For comparing results with different normalization, it would be convenient to introduce a non-dimensional quantity $\tilde{S}_{nl}(\omega)$ which is defined by $\tilde{S}_{nl}(\omega) = S_{nl}(\omega)/E^3 g^{-4} \omega_p^8$ and $\tilde{T}_1(\omega)$ likewise defined in terms of $T_1(\omega)$. As $g = 1$ and $\omega_p = 1$ in our numerical simulations, $\tilde{T}_1(\omega) = T_1(\omega)/E^3$. According to the result shown in figure 8, $-21 \leqslant \tilde{T}_1(\omega) \leqslant 30$ for both $E = 0.003$ and $E = 0.004$. RP91 evaluated $S_{nl}(f)$ when $\alpha = 0.01$, $f_p = 0.3\,\mathrm{Hz}$. Figure 2(a) of their paper indicates that they obtained $-2.3 \times 10^{-5} \leqslant S_{nl}(f) \leqslant 3.4 \times 10^{-5}$. Since $E = 0.305 \alpha g^2 \omega_p^{-4}$ for the JONSWAP spectrum as (2.34) indicates, and $S_{nl}(\omega) = S_{nl}(f)/2\pi$, the corresponding range of $\tilde{S}_{nl}(\omega)$ is $-17 \leqslant \tilde{S}_{nl}(\omega) \leqslant 25$. Thus the nonlinear energy transfer $T_1(\omega)$ obtained by the present direct simulation is about 20% larger than Hasselmann's $S_{nl}(\omega)$ as evaluated by RP91. Judging from the dispersion among different runs such as that shown in figure 7, which is rather large especially around the peak of the spectrum, a discrepancy of this magnitude seems to be acceptable.

3.4.2. *P-M spectrum*

We have also performed a similar series of simulations for the P-M spectrum. Figure 9 is the same as figure 7 except that the initial spectrum is given by the P-M spectrum with $E = 0.0035$ instead of the JONSWAP spectrum. The average is shown in figure 10, where the average of sixteen runs with $E = 0.002$ is also shown. According to (2.33), $E = 0.002$ and $E = 0.0035$ correspond to $\alpha = 0.01$ and $\alpha = 0.0175$, respectively. It can be confirmed that our $T_1(\omega)$ as plotted in figure 10 has succeeded in reproducing important characteristics of Hasselmann's $S_{nl}(\omega)$ again, such as (i) the existence of the positive maximum at $\omega \approx 1.0$, i.e. the frequency right at the peak of $\Psi(\omega)$, (ii) the existence of minimum at $\omega \approx 1.5$ which is slightly larger in

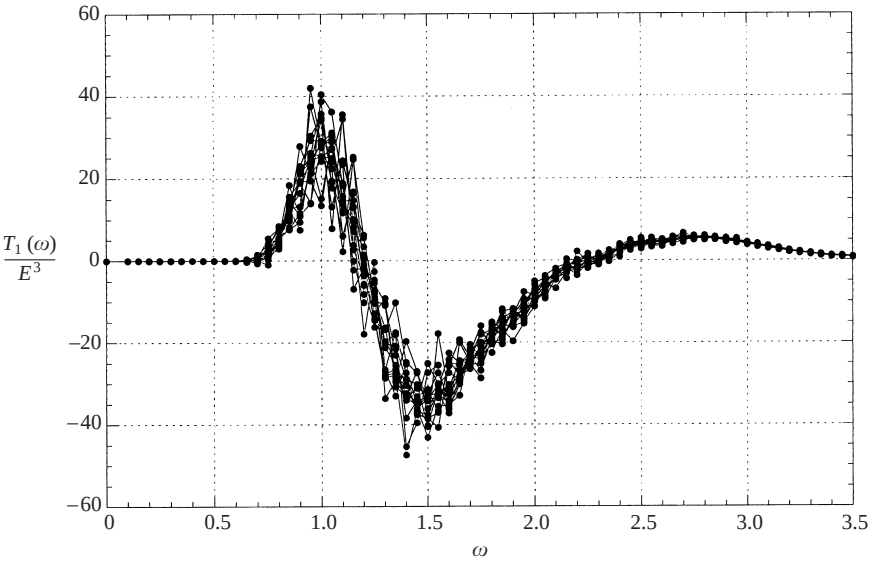

FIGURE 9. $T_1(\omega)/E^3$ obtained from 16 runs with the P-M spectrum, $E = 0.0035$.

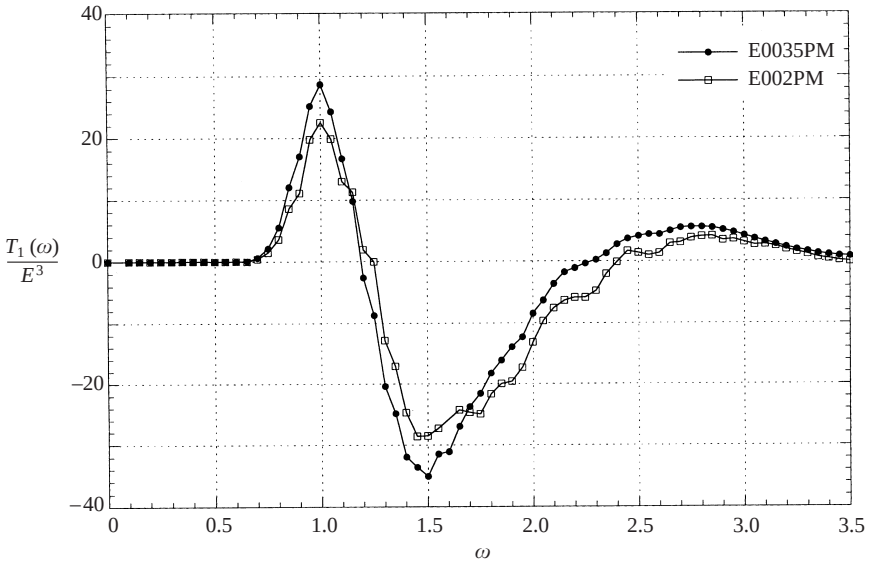

FIGURE 10. Average $T_1(\omega)/E^3$ for the P-M spectrum, $E = 0.002$ and 0.0035.

magnitude than the positive peak at $\omega \approx 1.0$, and (iii) a change of sign from negative to positive at $\omega \approx 2.5$.

In spite of such a favourable agreement in the overall pattern, the quantitative agreement between $S_{nl}(\omega)$ and $T_1(\omega)$ is rather disappointing. According to figure 10, $-29 \leqslant \tilde{T}_1(\omega) \leqslant 23$ for $E = 0.002$, and $-35 \leqslant \tilde{T}_1(\omega) \leqslant 29$ for $E = 0.0035$. On the other hand, RP91 obtained $-6.4 \times 10^{-6} \leqslant S_{nl}(f) \leqslant 6.4 \times 10^{-6}$ for the P-M spectrum with $\alpha = 0.01$, $f_p = 0.3\,\mathrm{Hz}$ as shown in their figure 2(*c*). Since $E = 0.2\alpha g^2 \omega_p^{-4}$ for the P-M spectrum as indicated by (2.34), the corresponding range of $\tilde{S}_{nl}(\omega)$

is $-17 \leqslant \tilde{S}_{nl}(\omega) \leqslant 17$. Thus our $T_1(\omega)$ is from 35% to even 100% larger than Hasselmann's $S_{nl}(\omega)$ as evaluated by RP91.

All of our computations have been performed within a rectangle $-15 \leqslant k_x \leqslant 15$, $-7.5 \leqslant k_y \leqslant 7.5$ on the $\boldsymbol{k}$-plane as explained in § 3.1. Then the maximum realizable frequency is about $4.1\omega_p$. Comparison between figures 8 and 10 indicates that, when E is the same, the energy transfer in the high-frequency region is much more vigorous for the P-M spectrum than for the JONSWAP spectrum. In this sense, the numerical computation for the P-M spectrum is more vulnerable to the truncation of the $\boldsymbol{k}$-plane. In figure 10, the curve for $E = 0.0035$ appears to be shifted to the left (i.e. to the lower frequency) compared to that for $E = 0.002$, and this probably suggests that the numerical results for the P-M spectrum have been influenced by the wavenumber cut off, especially when E is larger. Due to the vigorous energy flux towards the high-frequency region, simulations with the P-M spectrum are more liable to numerical overflow than those with the JONSWAP spectrum. Part of the energy which is transfered to the high-frequency region gradually piles up along the periphery of the truncated $\boldsymbol{k}$-plane, aggravates the truncation itself, and finally leads to numerical overflow. In the actual situation, this overflow would be replaced by some dissipative processes such as breaking.

There would be two ways to avoid this troublesome influence of the wavenumber cutoff, and consequently enable us to obtain a better estimate for $T_1(\omega)$ which is nicely scaled by E^3 as we have obtained for the JONSWAP spectrum. The first way would be to extend the rectangle on the $\boldsymbol{k}$-plane. However, with the limitation of our computational environment, this extension requires us to use a coarser mesh on the $\boldsymbol{k}$-plane, which would inevitably deteriorate the estimate of $\Psi(\omega)$ and hence that of $T_1(\omega)$. The second way would be to perform simulations with much smaller E. As the result with $E = 0.002$ in figure 10 shows much better agreement with $S_{nl}(\omega)$ than that with $E = 0.0035$, this way appears to be promising at first sight. However, since the rate of change of $\Psi(\omega)$ is proportional to E^3, the interval of time which is necessary for $\Psi(\omega)$ to show a change which is large enough to be detected with sufficient accuracy increases as $1/E^3$, and this interval of time would become unaffordably long for our computational environment if E needs to be decreased further than the present values. Thus neither way appears to be practical for us at the moment.

3.5. *Two-dimensional transfer* $T_2(\omega, \theta)$

The directional spectrum $\Phi(\omega, \theta)$ with resolutions $\Delta\omega$ and $\Delta\theta$ may be estimated similarly by

$$\Phi(i\Delta\omega, j\Delta\theta) \approx \sum_{k,l}{}'' \omega_{k,l}|b_{k,l}|^2 \Big/ \Delta\omega\Delta\theta, \tag{3.11}$$

where $\sum_{k,l}{}''$ denotes summation over pairs of mode numbers (k, l) that satisfy

$$(i - \tfrac{1}{2})\Delta\omega \leqslant \omega_{k,l} < (i + \tfrac{1}{2})\Delta\omega \quad \text{and} \quad (j - \tfrac{1}{2})\Delta\theta \leqslant \theta_{k,l} < (j + \tfrac{1}{2})\Delta\theta. \tag{3.12}$$

By evaluating $\Phi(\omega, \theta)$ at two different times, t_1 and t_2 say, we can obtain an estimate for the two-dimensional nonlinear energy transfer $T_2(\omega, \theta)$ by

$$T_2(\omega, \theta) = \frac{\Phi(\omega, \theta, t_2) - \Phi(\omega, \theta, t_1)}{t_2 - t_1}. \tag{3.13}$$

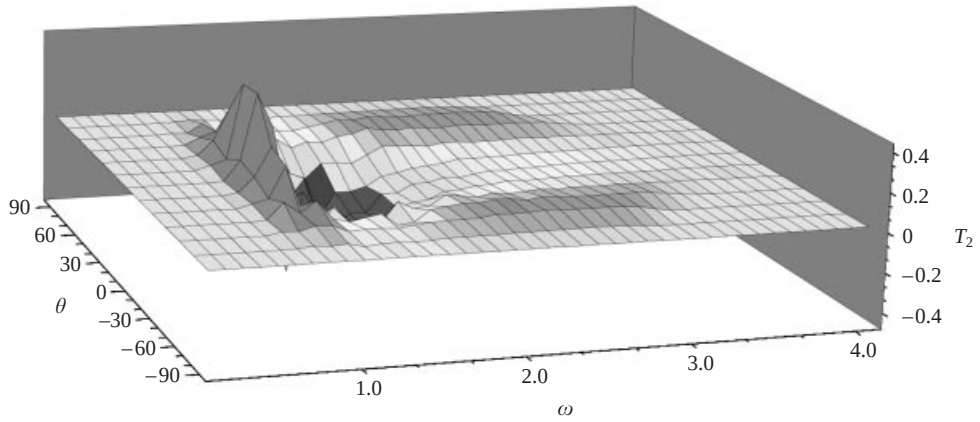

FIGURE 11. Surface plot of $T_2(\omega, \theta)$ for the JONSWAP spectrum: case[E005J_1].

This corresponds to the first method which we used to estimate $T_1(\omega)$. A method corresponding to the second method for estimating $T_1(\omega)$ is also possible, but we do not employ it here.

Figure 11 shows the surface plot of $T_2(\omega, \theta)$ thus obtained for a case with a JONSWAP spectrum with a $E = 0.005$. Here we tentatively fix $\Delta\omega = 0.1$, $\Delta\theta = 15°$. The pattern as a whole again agrees quite well with Hasselmann's $S_{nl}(\omega, \theta)$ as evaluated by previous authors. Particularly we can observe that the pair of ridges centred at $(\omega, \theta) \approx (2.4, \pm 50°)$ and elongated along the ω-axis, which is one of the remarkable features of $S_{nl}(\omega, \theta)$, has been successfully reproduced. Although not shown here, $T_2(\omega, \theta)$ for the P-M spectrum also shows such a fair agreement with $S_{nl}(\omega, \theta)$ at least as far as their qualitative patterns are concerned.

4. Conclusions and discussion

We have verified Hasselmann's theory for the nonlinear energy transfer among surface gravity waves by direct numerical simulations of the primitive equations for surface gravity waves. It has been confirmed that the nonlinear transfer can be scaled by E^3 as suggested by Hasselmann (1962) even when the effects of non-resonant interactions are taken into account.

According to the derivation of Hasselmann's S_{nl} from the Zakharov equation, the effect of non-resonant interactions vanishes as a result of integration with respect to t over a time scale which is much longer than $(ak)^{-2}$, or E^{-1}. At first sight, this appears to imply that Hasselmann's S_{nl} gives the long-term average of the rate of change of $\Psi(\omega)$, and that the rate of change of $\Psi(\omega)$ which is obtained from an evolution for much shorter times such as those treated here would differ from S_{nl}, because the lower-order non-resonant interactions could make an even larger contribution than the four-wave resonant interactions to such a short-term evolution.

But our numerical results indicate clearly that the rate of change of $\Psi(\omega)$ is given by Hasselmann's S_{nl} not only in the sense of long-term average but also at every instant of time. If this were not the case, it would be impossible to forecast the wave field 24 hours or 48 hours later by integrating the kinetic equation (1.5) or the energy balance equation (1.3) step by step with a short step size such as a few minutes.

So what has eliminated the effect of non-resonant interactions from the short-term evolution obtained by direct numerical simulations of the primitive equations? It is

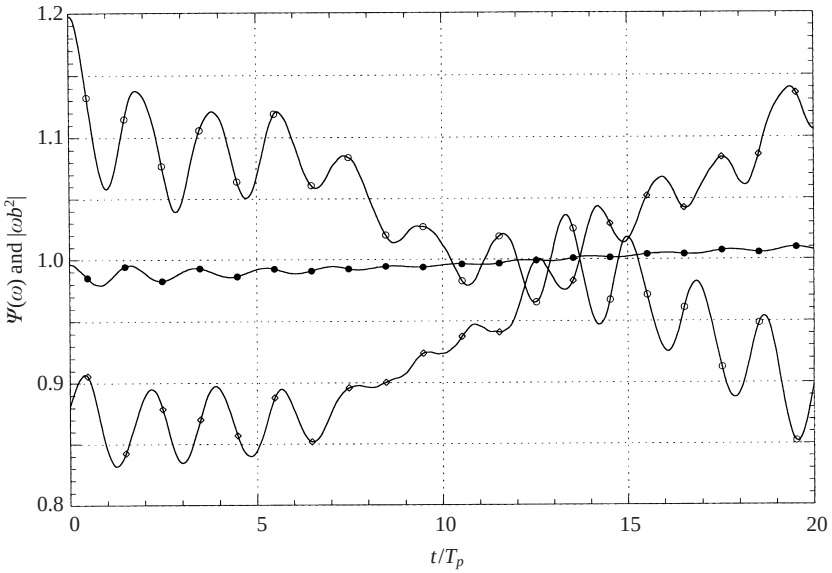

FIGURE 12. Comparison between $\Psi(\omega)$ and the energy of selected component waves. ●, $\Psi(\omega)$ with $\omega = 0.95$; ○, ◇, $\omega_{\boldsymbol{k}}|b_{\boldsymbol{k}}|^2$ of two selected modes with $\omega \approx 0.95$, case[E005J_1].

the averaging among modes on the $\boldsymbol{k}$-plane which is used to estimate the spectrum. As explained in § 3, we have estimated $\Psi(\omega)$ and $\Phi(\omega, \theta)$ by taking the average of many component waves on the $\boldsymbol{k}$-plane as their definitions (3.8) and (3.11) indicate, and through this averaging process all those contributions that depend explicitly on the phase relations between component waves have been cancelled out. Thus the effect of non-resonant interactions has disappeared not as a result of long-term integration in t, as the derivation of the kinetic equation (1.5) suggests, but as a result of averaging on the $\boldsymbol{k}$-plane. This averaging on the $\boldsymbol{k}$-plane has enabled us to detect the slow trend in the evolution of the spectrum in such a short time as just a few tens of characteristic periods.

To show the efficiency of the averaging on the $\boldsymbol{k}$-plane in removing the effect of non-resonant interactions, we plot in figure 12 the evolution of $\Psi(\omega, t)$ with $\omega = 0.95$ and the energy $\omega_{\boldsymbol{k}}|b_{\boldsymbol{k}}|^2$ of two adjacent modes which fall in the same bin $0.95 - \Delta\omega/2 \leqslant \omega < 0.95 + \Delta\omega/2$ when $\Psi(\omega, t)$ is estimated. All quantities have been divided by their respective averages over $0 \leqslant t \leqslant 20T_p$ to facilitate the comparison of their variability. It can be observed clearly that the large oscillations in the energy of component waves, which have been brought about by non-resonant interactions dominated by three-wave processes, have been removed quite efficiently by the averaging, and that the resultant spectrum $\Psi(\omega, t)$ behaves almost monotonically except for the first few periods, showing only the slow and irreversible trend which we are trying to detect.

We are aware that we have not proved if the spectrum estimated by the averaging on the $\boldsymbol{k}$-plane is equivalent to the spectrum defined by ensemble averaging, and that, in a strict sense, only the latter is supposed to obey the kinetic equation (1.5) in its evolution in time. In reality, however, we usually have only a single but huge realization, i.e. the actual wave field in the part of the ocean that we are interested in, and the forecast based on (1.5), or (1.3) in more realistic situations, would be entirely hopeless if the spectrum estimated for a single but huge realization by the averaging

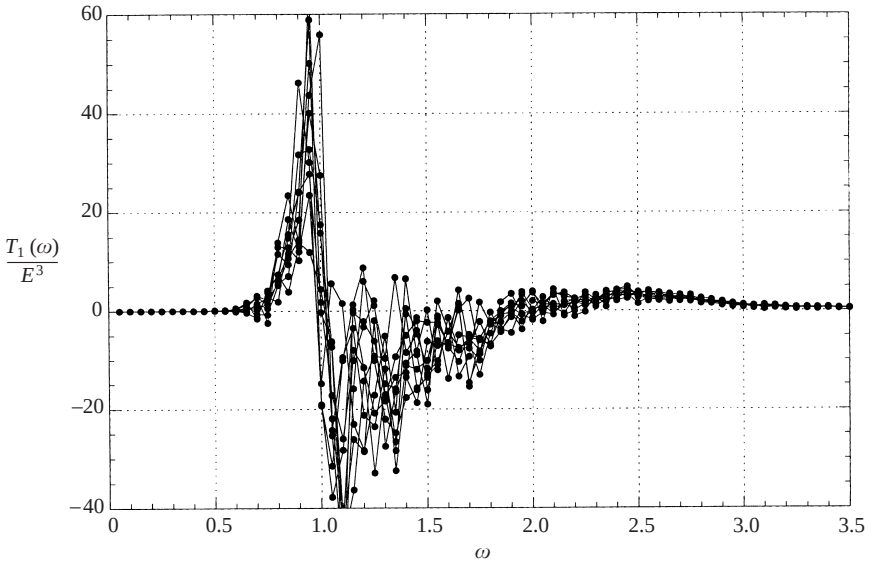

FIGURE 13. $T_1(\omega)/E^3$ obtained from 10 low-resolution runs with JONSWAP spectrum, $E = 0.005$.

on the $\boldsymbol{k}$-plane differs significantly from the spectrum defined by ensemble averaging. The problem of the evolution of the spectrum defined by the averaging on the $\boldsymbol{k}$-plane might be investigated more systematically by the approach developed by Rasmussen & Stiassnie (1999) and Stiassnie (2001).

Since the spectra are estimated by averaging on the $\boldsymbol{k}$-plane, the statistical reliability of our results critically depends on the density of modes on the $\boldsymbol{k}$-plane. Referring to figure 7, all the realizations give an almost identical result for larger ω where the statistical degrees of freedom is larger and hence the spectral estimate is more reliable. If we carry out the same analysis while reducing the density of modes on the $\boldsymbol{k}$-plane to about $1/10$, we obtain instead a result shown in figure 13. It can be observed clearly that the increase of the density of modes has greatly reduced the dispersion among runs. By extrapolating this result, we believe that it would be possible to get quite a reliable estimate for $T_1(\omega)$ from even a single realization, provided the density of modes on the $\boldsymbol{k}$-plane is large enough.

Recently Annenkov & Shrira (2001) have developed a new approach to numerical modelling of water wave evolution based on the Zakharov equation and, as an application of that, studied the transition to chaos of gravity waves. They found that two initially close points in the phase space, each corresponding to one wave field, diverge exponentially like $\exp(\lambda t)$ with $\lambda \approx (ak)^2$. From this fact, they concluded that a wave field with $ak \approx 0.1$, typical of oceans, loses all the information on the initial conditions over the time of the order of $O(10^3)$ characteristic wave periods. Because complete loss of information on the initial condition is generally required for the statistical description of the wave field, as well as the kinetic equation (1.5) which it gives, to be applicable, their finding appears to imply that it would be hopeless to try to detect a nonlinear energy transfer S_{nl} in (1.5) by numerical simulations which follow the evolution of the wave field only for a few tens of periods. However, the success of our approach in detecting the nonlinear transfer such as that shown in figure 8 proves that this is not the case. Further investigation is necessary to clarify the relation between these two results.

In all the computations discussed in this paper, we have truncated the nonlinear interactions at the four-wave processes by setting $M = 3$ in HOSM. So it would be desirable to assess quantitatively the contributions from higher-order nonlinear interactions which have been neglected from the outset. Unlike for more analytical approaches such as those based on the higher-order Zakharov equations (Krasitskii 1994; Stiassnie & Shemer 1984), it is quite easy for our numerical approach to take into account those higher-order nonlinear interactions. Actually it can be achieved just by changing M in the programme from 3 to some larger integer. Although this increase of M requires larger storage and longer CPU time, no essential difficulty is expected. We would like to investigate this in the future when our computational circumstance is improved.

Another interesting aspect of the problem which we have not treated in this work is the effect of finite water depth. Unlike the infinite depth case where Hasselmann's theory for nonlinear energy transfer as well as the weak turbulence thoery by Zakharov and his colleagues appear to be supported unanimously, the situation seems much more complicated, and there remain various things to be clarified further. One such problem would be the relative importance of the non-resonant three-wave process and the resonant four-wave process. As the water depth decreases and the dispersion gets weaker, it is expected that the lower-order non-resonant interactions begin to play more and more important roles in the evolution of the spectrum than in the deep-water case. Moreover Zakharov (1999) argues that the validity of the weak turbulence theory itself might be strictly limited when the water becomes shallow. The programme based on HOSM can be adapted to the case of finite depth quite easily, and has been applied successfully to various finite-depth problems (e.g. Tanaka 1993). Direct numerical simulations of the primitive equations based on HOSM would certainly be quite promising as a method of studying the dynamics of fields of surface gravity waves in finite-depth or shallow water.

The author would like to express his cordial thanks to Professor A. Masuda, Professor W. Perrie, Dr K. Komatsu and Dr H. Schaeffer for their valuable advice and comments. It is also gratefully acknowledged that discussion with Professor V. Shrira has been very valuable and stimulating. His various comments on the first draft have been helpful in revising the manuscript. This work was partially supported by a Grant-in-Aid for Scientific Research from the Ministry of Education, Science and Culture. It was also partially supported by a grant from the Research Foundation for the Electrotechnology of Chubu (REFEC).

REFERENCES

Annenkov, S. & Shrira, V. I. 2001 On the predictability of evolution of surface gravity and gravity-capillary waves. *Physica D*, **152–153**, 665–675.

Bendat, J. S. & Piersol, A. G. 1986 *Random Data*. John Wiley & Sons.

Canuto, C., Hussaini, M.Y., Quarteroni, A. Q. & Zang, T. A. 1988 *Spectral Methods in Fluid Dynamics*. Springer.

Dommermuth, D. G. 2000 The initialization of nonlinear waves using an adjustment scheme. *Wave Motion* **32**, 307–317.

Dommermuth, D. G. & Yue, D. K. P. 1987 A high-order spectral method for the study of nonlinear gravity waves. *J. Fluid Mech.* **184**, 267–288.

Dyachenko, A. I. & Lvov, Y. V. 1995 On the Hasselmann and Zakharov approaches to the kinetic equations for gravity waves. *J. Phys. Oceanogr.* **25**, 3237–3238.

Hasselmann, K. 1962 On the non-linear energy transfer in a gravity-wave spectrum. Part 1. General theory. *J. Fluid Mech.* **12**, 481–500.

HASSELMANN, S. & HASSELMANN, K. 1981 A symmetrical method of computing the nonlinear transfer in a gravity-wave spectrum. *Hamburger Geophys. Einzelschr.* A52.

KARTASHOVA, E. 1998 Wave resonances in systems with discrete spectra. In *Nonlinear Waves and Weak Turbulence* (ed. V. E. Zakharov), pp. 95–129. American Mathematical Society.

KOMATSU, K., KUSABA, T. & MASUDA, A. 1993 An efficient method for computing nolinear energy transfer among wind waves. *Bull. Res. Inst. Appl. Mech., Kyushu Univ.* **75**, 121–146 (in Japanese).

KOMATSU, K. & MASUDA, A. 1996 A new scheme of nonlinear energy transfer among wind waves: RIAM method – Algorithm and Performance – *J. Oceanogr.* **52**, 509–537.

KRASITSKII, V. P. 1994 On reduced equations in the Hamiltonian theory of weakly nonlinear surface waves. *J. Fluid Mech.* **272**, 1–20.

MASUDA, M. 1980 Nonlinear energy transfer between wind waves. *J. Phys. Oceanogr.* **10**, 2082–2093.

NEWLAND, D. E. 1993 *An Introduction to Random Vibrations, Spectral & Wavelet Analysis.* Longman.

RASMUSSEN, J. H. & STIASSNIE, M. 1999 Discretization of Zakharov's equation. *Eur. J. Mech.* B/*Fluids* **18**, 353–364.

RESIO, D. & PERRIE, W. 1991 A numerical study of nonlinear energy fluxes due to wave-wave interactions. Part 1. Methodology and basic results. *J. Fluid Mech.* **223**, 603–629 (referred to herein as RP91).

STIASSNIE, M. 2001 Nonlinear interactions of inhomogeneous random water waves. Preprint.

STIASSNIE, M. & SHEMER, L. 1984 On modifications of the Zakharov equation for surface gravity waves. *J. Fluid Mech.* **143**, 47–67.

STUART, A. & ORD, K. 1994 *Kendall's Advanced Theory of Statistics. Vol. 1 Distribution Theory.* Edward Arnold.

TANAKA, M. 1993 Mach reflection of a large amplitude solitary wave. *J. Fluid Mech.* **248**, 637–661.

TANAKA, M. 2001 A method of studying nonlinear random field of surface gravity waves by direct numerical simulation. *Fluid Dyn. Res.* **28**, 41–60.

WEST, B. J., BRUECKNER, K. A., JANDA, R. S., MILDER, M. & MILTON, R. L. 1987 A new numerical method for surface hydrodynamics. *J. Geophys. Res.* **92**, 11803–11824.

YUEN, H. C. & LAKE, B. M. 1982 Nonlinear dynamics of deep-water gravity waves. *Adv. Appl. Mech.* **22**, 67–229.

ZAKHAROV, V. E. 1968 Stability of periodic waves of finite amplitude on the surface of a deep fluid. *J. Appl. Mech. Tech. Phys.* (Engl. Transl.) **2**, 190–194.

ZAKHAROV, V. E. 1999 Statistical theory of gravity and capillary waves on the surface of a finite-depth fluid. *Eur. J. Mech.* B/*Fluids* **18**, 326–344.

ZAKHAROV, V. E., L'VOV, V. S. & FALKOVICH, G. 1992 *Kolmogorov Spectra of Turbulence I – Wave Turbulence.* Springer.

ZHAO, D.-L., KOMATSU, K., KUSABA, T. & MASUDA, A. 1996 An experiment on wind waves in decay area in reference to the role of nonlinear energy transfer. *Rep. Res. Inst. Appl. Mech., Kyushu Univ.* **41**, 1–14.